Distinct neural patterns enable grasp types decoding in monkey dorsal premotor cortex

Yaoyao Hao, Qiaosheng Zhang, Marco Controzzi, Christian Cipriani, Yue Li, Juncheng Li, Shaomin Zhang, Yiwen Wang, Weidong Chen, Maria Chiara Carrozza, Xiaoxiang Zheng

Title: Distinct neural patterns enable grasp types decoding in monkey dorsal premotor cortex

Abbreviated title: Grasp patterns in PMd

Author names and affiliations: Yaoyao Hao[1], Qiaosheng Zhang[1], Marco Controzzi[2], Christian Cipriani[2], Yue Li[1], Juncheng Li[1], Shaomin Zhang[1], Yiwen Wang[1], Weidong Chen[1], Maria Chiara Carrozza[2*], Xiaoxiang Zheng[1*]

[1] Qiushi Academy for Advanced Studies, Zhejiang University, Hangzou, 310027, China

[2] The BioRobotics Institute, Scuola Superiore Sant'Anna, Pontedera, 56025, Italy

***Corresponding author**: Xiaoxiang Zheng (Address: Mail Box 1536#, Qiushi academy for advanced studies, Zhejiang University, 38 Zheda Road, Hangzhou, Zhejiang Province, 310027, China. E-mail: zxx@mail.bme.zju.edu.cn) and Maria Chiara Carrozza (Address: The BioRobotics Institute, Scuola Superiore Sant'Anna, V.le Rinaldo Piaggio 34, Pontedera, 56025, Italy. E-mail: chiara.carrozza@sssup.it)

Number of pages: 36

Number of figures, tables, multimedia and 3D models: 9, 0, 0 and 0, respectively

Number of words for Abstract, Introduction, and Discussion: 249, 499 and 1492, respectively

Contents of supplemental material: none

Conflict of Interest: none

Acknowledgements: This research was supported by National Key Basic Research Program of China (2013CB329506), Programme for Scientific and Technological Cooperation between Italy-China (2013-2015), National High Technology Research and Development Program of China (2012AA011602), National Natural Science Foundation of China (No. 61031002, 61001172, 61003150).

Abstract

Recent studies have shown that dorsal premotor cortex (PMd), a cortical area in the dorsomedial grasp pathway, is involved in grasp movements. However, the neural ensemble firing property of PMd during grasp movements and the extent to which it can be used for grasp decoding are still unclear. To address these issues, we used multielectrode arrays to record both spike and local field potential signals in PMd in Macaque monkeys performing reaching and grasping of one of four differently shaped objects. Single and population neuronal activity showed distinct patterns during execution of different grasp types. Cluster analysis of neural ensemble signals indicated that the grasp related patterns emerged soon (200-300 ms) after the go cue signal, and faded away during the hold period. The timing and duration of the patterns varied depending on the behaviors of individual monkey. Application of support vector machine model to stable activity patterns revealed classification accuracies of 94% and 89% for each of the two monkeys, indicating a robust, decodable grasp pattern encoded in the PMd. Grasp decoding using local field potentials, especially the high-frequency bands, also produced high decoding accuracies. This study is the first to specify the neuronal population encoding of grasp during the time course of grasp. We demonstrate high grasp decoding performance in PMd. These findings, combined with previous evidence for reach related modulation studies, suggest that PMd may play an important role in generation and maintenance of grasp action and may be a suitable locus for brain-machine interface applications.

Introduction

Reaching to grasp different kinds of objects is one of the most important and fundamental functions in our daily life. Successful grasping requires: (1) transforming visual properties of target objects into appropriate arm and hand configurations, (2) executing these configurations to control guidance of arm movements and shaping of hand movements and (3) real time adjustments of these configurations based on biomechanical interactions between hand and object (Davare et al., 2011). Many cortical areas including visual, posterior parietal, frontal motor and somatosensory areas are involved in grasp operations (Brochier and Umilta, 2007; Gardner et al., 2007). Previous functional and anatomical studies have proposed division of these cortical areas into two grasp networks: a dorsolateral network for grasp control, which involves the classic grasp pathway between anterior intraparietal (AIP) and ventral premotor cortex (PMv, area F5), and a dorsomedial one for reaching, which is coordinated by area V6A with strong connections to medial intraparietal (MIP) and dorsal premotor cortex (PMd, area F2) (Galletti et al., 2003; Rizzolatti and Matelli, 2003; Grafton, 2010).

PMd, an area in dorsomedial pathway, has been traditionally viewed as part of the reach-related system. PMd contains neurons highly modulated by parameters of reach in a goal-directed grasp (Caminiti et al., 1991; Fu et al., 1993; Wise et al., 1997; Messier and Kalaska, 2000). However, recent developments have shown this area to be also related to distal hand grasp movement. Initial studies on the functional properties of PMd neurons for grasp movement showed high selectivity for specific grip type and wrist orientation during both planning and execution of grasp (Raos et al., 2003; 2004), not dissimilar to neurons in PMv (Murata et al., 1997; Raos et al., 2006). Based on intracortical microstimulation, spike recording and multiunit correlation studies, It has also been demonstrated that PMd neurons are specific for grasp types (different objects presented), grasp

dimensions, or grasp force (Raos et al., 2004; Stark and Abeles, 2007; Stark et al., 2008; Hendrix et al., 2009). A functional magnetic resonance imaging study indicated that PMd is involved in processing visuospatial parameters (object slant) for grasping (Verhagen et al., 2008). Another study demonstrated an inhibitory role of PMd in grip force control during a precision grasping and lifting task (van Nuenen et al., 2012). Thus, the evidence suggests some role for grasp-specific neuron activity in PMd.

Despite these many studies, no study has systematically investigated the ensemble firing properties and grasp decoding characteristics of neuronal population activity in PMd. In this study, we use multielectrode recording methods in PMd of monkeys trained to reach and grasp four different objects. We examined the single and population neuronal firing properties and applied clustering analysis to investigate the grasp discrimination along the time course of grasp. Based on both spike and local field potential signals, we find the ensemble firing pattern to be reliable during the time course of grasp and we were able to decode four kinds of grasp movement. These results indicate that PMd area is a great candidate as implantation site of invasive brain machine interfaces for neuroprosthetic.

Materials and Methods

Behavioral setup and tasks

Two monkeys (rhesus macaque, male), named B03 and B04, were trained to reach and grasp four objects attached to a panel in front of them, using their dominant hand (right hand for B03 and left hand for B04). As shown in Fig 1A, the objects were fixed on the center of a transparent board, which was located vertically in front of the animal at the chest level. The monkey was seated in a primate chair with head fixed and arms resting on clapboard at chest level. The distance from the board to the eyes of the animal was approximately 50 cm. A PC-controlled LCD monitor, mounted behind the board, illuminated the object when the corresponding screen area behind the object was lit to instruct the monkey to grasp (light on) or release (light off) the object. The four objects used in this experiment, have been selected with appropriate shapes, in order to induce a specific hand postures to the monkeys. These are shown in Fig 1B and shaped as follow: a cylinder (ø = 18 mm; l = 100 mm), a plate (5 mm × 60 mm × 120 mm), a small cone ($ø_b$ = 10 mm; l = 30 mm) and a small ring ($ø_i$ = 25 mm; $ø_o$ = 30 mm). Each object can be mounted on or removed from the board easily by a transparent pedestal adhered to the object. The cylinder, plate and ring were fixed to the board with their longer axes vertical to the ground; the cone was placed with its base facing the board. These fixed positions have been selected in order to force the monkey to adopt the same wrist orientation during the grasping of the objects presented. The corresponding hand postures required the monkey to pose on each object are also shown in Figure 1B, which are (1) power grip for the cylinder (with fingers and thumb flexing around the object, against the palm), (2) primitive precision for the plate (performed using the thumb in opposition to the glabrous surface of fingers' distal phalanges), (3) two-finger hook grip for the ring (with index and middle fingers inserted into the

ring) and (4) lateral for the cone (performed using the thumb and the radial surface of the last phalanx of the index finger).

As shown in Figure 1C, a trial was initiated after the object was illuminated by the light projected from the background screen (hereafter referred to as Light ON) and the monkey was required to reach and grasp the object using the proper prehensile pattern and hold it for 1.5 to 2 seconds until the background light was turned off (hereafter referred to as Light OFF). The monkey was trained to release the object and return the hand to the rest position after Light OFF. Completion of a successful trial resulted in several drops of water reward. In each session, four objects, each presented for ~50 trials, were presented in the same position to the monkey in a randomized order. Any unsuccessful trial, either with wrong grasp type or wrong grasp timing, was excluded from further analysis. To facilitate analysis, we partitioned the period of each trial into the following phases: (1) *resting*, when the monkey rested his arm on the clapboard; (2) *reaching* and *grasping*, during which the monkey reached the object and formed a grip; (3) *holding*, during which the monkey held the object for 1.5 to 2 seconds; (4) *releasing*, during which the monkey opened its hand, released the object and withdrew his arm. All the procedures were controlled by custom-developed software. Hand and arm movements were also recorded using an infrared camera during the experiment.

Figure1

Surgical implantation and neural recording

Neural data were collected from Utah microelectrode arrays (Blackrock Microsystems, USA, 96 channels, 4.2 ×4.2 mm) chronically implanted in the hand area of dorsal premotor cortex (PMd) contralateral to the hand performing the task (left for B03 and right for B04). The implantation sites

were identified by the *sulcus* landmarks, i.e. PMd site was dorsal to the spur of arcuate *sulcus*, separating it from ventral premotor cortex (Raos et al., 2004; Hoshi and Tanji, 2006). The position of the implantation was further confirmed by intracortical microstimulation (ICMS, 11-44 pulses, 200 μs width, 333 Hz, 5-90 μA) applied to each electrode. In both Monkeys, a percentage of sites (31.25% and 10.42%) elicited obvious distal or wrist movement. In addition, two head posts were placed on the skull for head stabilization and array connector fix, respectively. The surgical procedures were similar to those previous described by Zhang et al (2012). The monkey was allowed to recover from surgery for at least one week, during which, antibiotics (Ceftriaxone sodium, 1 g/day) were administered. Before this task, B03 had been enrolled in a center-out experiment for several months and the neural data used in the present work were recorded about one year after the implantation. B04 was naïve before this task and the neural signal was recorded one month after implantation. All experimental procedures in this study conformed to the Guide for the Care and Use of Laboratory Animals (China Ministry of Health) and related European directives (2010/63/EU).

Neural recordings were obtained from the microelectrode array in PMd using a Cerebus data acquisition system (Blackrock Microsystems, USA). Analog signals from each channel were amplified, filtered (Butterworth bandpass, 0.3-7500 Hz), and digitized (14 bit resolution, 30 kHz sample). The signal was further digitally filtered (Butterworth highpass, at 250 Hz) for the detection of spike activity. Spike activity was detected by thresholding the filtered signal at a level of -5.5 times the root mean square (RMS) of baseline signal and sorted using predefined waveform templates. The signal was down sampled to 1 kHz and digitally filtered (Butterworth low-pass, at 500 Hz) in order to measure the Local Field Potentials (LFPs). The timing of behavior-related events,

including Light ON, Light OFF and reward, was also recorded via the digital input port of the system.

Grasp Pattern Visualization

Neural spikes from each electrode were resorted using commercial software (Offline Sorter, Plexon Inc., USA) session by session to isolate single units (Nicolelis et al., 2003). Signal-to-noise ratio (SNR) was assessed for each isolated unit by dividing the mean peak-to-peak voltage of the isolated unit by twice the standard deviation of the estimated noise (Suner et al., 2005). The spikes of each unit were counted for contiguous 100 ms bins across the entire trial. The baseline firing rates (500 ms before Light ON) in each trial were subtracted for each object to eliminate the object fixation activation (Raos et al., 2004) influence on the grasp action modulation. A unit was judged as tuned to the reach grasp movement if its firing rate in any bin during reach grasp movement was significantly different from the baseline firing rate (ANOVA, $p < 0.01$).

To visualize the PMd neuron ensemble firing patterns during different grasps, we used a manifold learning method, Laplacian Eigenmap (LE), to reduce the original high dimensional neural signals to a lower dimensional space. Compared to the traditional dimension reduction methods, e.g., principal component analysis, LE uses the differential manifold and spectrum graph theory and has the advantage of maintaining the structure of the manifold on which the nonlinear dynamics of data may reside (Van der Maaten et al., 2009). The LE method keeps the local neighbor characteristics of manifold on average, i.e., data points that are neighbors in high dimensional space should also be neighbors when they are mapped into lower dimensional space (Belkin and Niyogi, 2003). In this application, we reduced the neuronal firing dimensions to 3 and plotted them in 3-dimension along the time course of grasp.

Clustering and Decoding Analysis

In addition to single neuron activity we examined population activity during the reaching and grasping movements by characterizing the neural firing rates of all units across that trial. In each time bin, the firing rates of individual neurons formed a vector with each element corresponding to a unique isolated unit. Standardized Euclidian distances between a pair of vectors were calculated to measure the similarity between objects along the time course of grasp.

Based on the distance metric hierarchical cluster analysis was applied to determine the degree of object discrimination along the time course of reaching and grasping movement. Within each session, neural vectors of trials from each object were linked together in a hierarchical tree according to the vector distances. The two objects with closest distance were linked first. As objects were paired into binary clusters, the newly formed clusters were grouped into larger clusters until a hierarchical binary tree was formed. The evaluation of the resulting cluster model can be used to validate the neural pattern discrimination (i.e. if the vectors form the same object can be grouped together) along the time course of grasp movement. Thresholding the hierarchical tree can create a partition of the vectors and an arbitrary number of subgroups. A percentage of correctly sorted objects (Cs) along the time course t was calculated on the basis of the hierarchical tree (Brochier et al., 2004) as:

$$\mathrm{Cs(t)} = \frac{\mathrm{Gr_{max}} - \mathrm{Gr_{act}}}{\mathrm{Gr_{max}} - \mathrm{Gr_{min}}} \times 100\% \quad (1)$$

where $\mathrm{Gr_{act}}$ is the least number of groups in which only vector(s) from the same object were clustered; $\mathrm{Gr_{max}}$ is the maximum number of possible groups, which equals the total number of vectors; $\mathrm{Gr_{min}}$, which is 4 in our case, is the minimum number of groups when all the vectors from each object were correctly grouped together. Cs is 1 if all the objects are correctly grouped, implying a perfect discrimination of the neural firing patterns at that time bin and is 0 if none of the

vectors from the same objects are grouped together. It is important to notice that this evaluation method was strict, so we focused on the relative differences along the time course of reach grasp movement, rather than on the absolute magnitudes.

Four kinds of classification methods, both linear and nonlinear, comprising of fuzzy k-nearest neighbors (FKNN), probabilistic neural network (PNN), Fisher's linear discriminant analysis (LDA) and support vector machine (SVM) were implemented in order to evaluate whether the neural activity in PMd could be used to decode different grip types. The classifiers worked in a bin-wise decoding mode, i.e., every bin used in one trial was labeled as the object grasped in the training set. During testing the classifier computed a result label for each bin; the prevalent label in one trial (majority voting across the trial) was deemed the final label of the tested trial. Furthermore, the effects of different decoding window length, training length and number of neurons were also analyzed. All the algorithms and test procedures were implemented using MATLAB scripts. FKNN was custom developed according to (Keller et al., 1985). PNN and LDA were implemented using MATLAB built-in function *newpnn* and *ClassificationDiscriminant*. SVM was developed using open source library LIBSVM (Chang and Lin, 2011).

Local Field Potential analysis and decoding

The signal characteristics of LFP in frequency domain were extracted by estimating the power spectrum of all the frequencies using multitaper spectral analysis (Thomson, 2000). The power spectrum was calculated over a 300 ms window centered at each 100 ms time step, with a frequency resolution of 0.5 Hz, channel by channel. The 100 ms time step was chosen for being consistent with the spike analysis. LFP power was then normalized to zero mean and unit SD in each frequency band and the mean power of baseline subtracted (before Light ON). For further analysis, the LFP

power was divided into seven frequency bands, which were δ (0.3–5 Hz), θ-α (5–15 Hz), β (15–30 Hz), γ1 (30–50 Hz), γ2 (50–100 Hz), γ3 (100–200 Hz) and a broad high-frequency band (bhfLFP, 200–400 Hz) (Zhuang et al., 2010).

The SVM classifier was also employed to decode the four grasp types, using features of LFP power in different frequency bands. First, the power was summed up across all the frequencies in each frequency band. Second, one second data segment (10 bins after Light ON) was extracted across all the trials in each session and was randomly assigned to non-overlapping training and testing sets. The SVM classifier worked in a bin-wise model as in spike decoding; the most prevalent label in one trial was deemed the resulting label of that trial. A two-fold cross-validation was conducted 50 times for each session and each frequency band to evaluate the classification performance.

Results

Two monkeys were trained to perform reach and grasp of four objects. Simultaneous spike recordings and broadband LFP (0.3-500 Hz) from PMd were recorded in a total of 16 sessions distributed in one month (8 for each monkey, ~200 trials per session). After offline sorting, we isolated an average of 35 units (B03) and 57 units (B04) in each session, in which 86% and 93% had signal-to-noise ratio larger than 3.0 (see methods). The majority of these units (92% and 89%) showed significant differences in firing relative to the baseline for at least one bin during the movement (one-way ANOVA, $p < 0.05$) and were deemed as task-related. Neural firing pattern analysis and decoding were conducted to demonstrate the distinct grasp type related neural patterns and considerable classification effects in dorsal premotor cortex.

Neural property during reach and grasp

Example Single Units

Most of the task-related neurons (81% for B03 and 75% for B04) further showed grasp type selectivity during reaching to grasp movement as assessed by ANOVA (in the interval between Light ON and Light OFF event, at least one bin's firing rate to any one object is significantly different from one of the other objects, $p < 0.05$). Figure 2 shows some representative neurons from both monkeys B03 and B04. The firing rate was averaged across all the trials in one session for each object and was doubly aligned to Light ON (left) and Light OFF (right) events. Neuron 77-2 (channel 77, unit 2) from B03 first showed a slight decrease after *reaching* movement began, followed by an increase its firing to peak, a decline gradually during the *holding* period, and return to baseline following *release*. Although the temporal firing pattern was the same for the four grasp types, the amplitude of the firing during the *holding* period was dependent on grasp type, with

highest firing rate for the cylinder object and lowest for the small cone. Neuron 94-1 from B04 had a similar firing pattern with some exceptions. First, Neuron 94-1 had an earlier response than Neuron 77-2 (~100 ms vs. ~200 ms). According to the video recorded, we found that B04 was faster at achieving grasp than B03 after Light ON (B03: 385 ms ± 100 ms; B04: 235 ms ± 93 ms). Thus, the period during which the four movements could be discriminated in monkey B04 was shorter than for B03. These two differences were also true for most of the other neurons recorded in B04 (e.g. 94-2). Neuron 21-2 only responded to power grip of the cylinder, indicating selectivity to "whole-hand" involvement. Neuron 92-1 displays a rather broad selectivity, discharging strongly for the power grip, hook grip and primitive precision grip; the firing rate for lateral grip remained at baseline. The activity of this neuron could be related to the middle finger because the only difference between lateral grip and other grips is the involvement of middle finger. Neurons 91-1 and 94-2 from B04 had similar firing features among different grips as for the Neurons 21-2 and 92-1 from B03.

It is important to note that the different objects used in this study were located in the same position on the board, i.e., the arm reach direction was always the same across different objects. Thus, the firing differences were mainly a result of the different grip types. On the other hand, we also found some neurons sensitive only to reaching, showing no differences among different grasps as illustrated in the bottom panels in Figure.2. These two neurons responded to the reach movement in the form of either excitatory (Neuron 50-2) or inhibitory (Neuron 61-1) response modulation and displayed no significant difference in response between any of the objects. Consistent with other studies (Stark et al., 2007) these data suggest that both reaching and grasping neurons exist in area PMd.

Figure2

Ensemble Firing Pattern and Clustering

The ensemble representation of grip types at the population level was examined by calculating the pair wise distance of neural firing vectors between different objects (see Methods). The results in one representative session for each monkey are shown in Figure 3 as a color matrix. The distance between every possible pair of neural firing vectors during grasp of different objects is illustrated in pseudo color, with red representing the lowest levels of similarity and blue the highest. In the top panel of Figure 3 (monkey B03) we can see that the distance is shortest when the neural firing vectors are from the same object (the four distinguishable yellow/green square patterns along diagonal). In addition, the degree of similarity was also high between the plate and ring (oranges), plate and cone (oranges), indicating similar firing patterns while performing these two pairs of grasps. Monkey B04 also had the highest similarity within the same object and lowest similarity between different objects, as demonstrated in the bottom panel of Figure 3. Overall, these results suggest that the neural firing patterns in PMd were consistent for the same object and distinguishable between different grips.

Figure3

To further visualize the grasp patterns in 3D space, we applied Laplacian Eigenmaps (LE) algorithm to reduce the high dimensions of neural data into 3D space. Every neuronal firing vector along the time course of grasp was projected into a point (LE1, LE2, LE3) in the three dimensional space and formed a firing pattern trajectory for each trial. Distinct patterns among different grasps, which were represented by intra-class clustering and prominent inter-class discrimination, can be found in both monkeys (cf. Figure 4). After Light ON, each trial rotated anticlockwise along

different trajectories in the space, and formed a closed loop, indicating the firing pattern returned to pre-Light ON base line. For Monkey B03, the grasp of cylinder and cone were very distinct while the plate and ring had similar firing patterns and were not easy to distinguish. For Money B04, the grasp patterns showed greater differences across different phases of grasp movement after Light ON, although, in comparison to B03, there appears to be greater variability within each grasp type. Because the LE reduction method maintains the local neighbor characteristics, we can infer that the original neuronal ensemble firing has also the same distinct grasp dependent discrimination patterns.

Figure4

To quantify the motor selectivity of PMd grasping neurons and determine when the grasp types can be clearly discriminated from neural activities along the time course of grasp movement, unsupervised hierarchical clustering analysis and quantitative evaluation was conducted (see Methods). In each session, 10 trials from each object were randomly selected. A total of 40 neural firing vectors at each time bin were used to cluster and correctly sort objects; correct sorted percentage (Cs) was calculated bin by bin as the indicator of degree of object discrimination. Figure 5 shows the results averaged across all 8 sessions for each monkey. For monkey B03, the Cs values rose rapidly 300 ms after Light ON and reached a maximum 600 ms later; then it decreased to the baseline level 400 ms later. The period between 0.3 s and 1.3 s is the period with the most distinguishable information about different grips. B04 had the similar discriminating period, one that was earlier (200 ms vs. 300 ms) and shorter (0.2-0.8 s vs. 0.3-1.3 s) than B03. These periods of high discrimination roughly corresponded to the period of *reaching*, *grasping* and beginning of *holding* in both monkeys.

Together with the ensemble pattern analysis, we can draw conclusions from these observations that

(1) different grip patterns can be found in both ensemble and reduced neural activity in PMd; (2) the distinguishable patterns appeared soon (200-300 ms) after Light ON, during the time when the monkey was reaching towards the object. This indicates that the grasp information was encoded before the actual grasp execution, i.e., during preshaping; (3) in the *holding* period, although the monkey still held the object using different grips, the Cs values showed decreasing trends, indicating the discrimination of PMd neurons gradually declined during the static holding phase. Furthermore, the most distinguishable duration obtained for each monkey, during which the classifier was most reliable, can further be used to determine the shortest time period for decoding.

Figure 5

Decoding with spikes and LFPs

Spike Decoding and Analysis

To investigate the performance of hand grip types decoding in PMd, the fuzzy k-nearest neighbor (FKNN), probabilistic neural network (PNN), Fisher's linear discriminant analysis (LDA) and support vector machine (SVM) models, working in a bin-wised model, were used for offline classification. The models were trained and tested using the bins in the most distinguishable segments obtained in the cluster analysis for each monkey (i.e., 0.3-1.3 s vs. 0.2-0.8 s after Light ON for B03 and B04, respectively). To assess the classification accuracy, a two-fold cross-validation, randomly assigned with equal size data for train and test, was used and averaged 100 times in each session. The session-wise results using four decoding models are illustrated in Figure 6A. In both monkeys all the decoding accuracies were above chance level (25%) regardless of the decoding models. SVM resulted in the highest accuracy in both monkeys (an average of 94.2%, SD 3.5% for B03 and 88.6%, SD 3.3% for B04). The performance of B03 was better than B04 (ANOVA, $P <$

0.01). Due to its higher classification accuracy, we chose to use SVM as the only classifier for the following analysis.

Figure 6

To further explore how the decoding performance changed over the time course of grasp movement, we employed a sliding time window decoding approach. For each time point, the classifier was trained and tested only using the bins contained in a time window centered at the point. The time window moved point by point (i.e., bin by bin). The representative results of one example session using different time window lengths are shown in Figure 6B. The four time window lengths showed similar profiles. The accuracy substantially increased after Light ON, reached to a highest point about 700-1000 ms later and declined gradually near Light OFF. For the same time point, the accuracy increased with the window length and resulted in little difference when the length was larger than 700 ms. Taking 900 ms as the time window length, we got a reliable result (95% ± 1.9%) as early as 600 ms after Light ON. This period fell within the most distinguishable segments obtained by the cluster analysis above.

In order to achieve a more efficient decoding we tried to calculate the least number of trials and neurons required to train the classifier model. Figure 6C presents the classification accuracy as a function of training trial numbers per object. The accuracy increased with the number of trials used and reached a maximum with only 8 (for B03) and 11 (for B04) trials. It is also important to notice that the accuracies were still above chance level (77% for B03 and 56% for B04) with only a single trial training; this indicates a highly constant firing property between trials. Figure 6D showed the decoding performance as a function of the number of the PMd neurons used for the classifier. With the same number of neurons, monkey B03 always outperformed B04. Decoding accuracy reached

90% of the highest values using only 16/34 (B03) and 29/48 (B04) neurons, which indicates a redundant and robust grasp encoding in PMd area. A final important point is that, with sufficient number of neurons, both monkeys achieved comparable high accuracy. Overall, neural ensemble recordings in PMd provided good decoding performance using only a small number of training trials and small number of neurons.

Figure 7

In order to reveal the misclassifications of individual objects, confusion matrices (CMs) of target objects versus predicted objects are presented in Figure 7 both in trial and bin wise models (see Methods). The trial-wise CM in Figure 7A shows high classification accuracies for each object (high values along diagonal) except for the Cone that was misclassified mainly as the ring at an average level of 13%. The bin-wise CM in Figure 7B also confirmed the misclassification from Cone to Ring. Additionally, the confusion between Cylinder and Plate was further revealed in this bin-wise CM, indicating that these two kinds of grasp types were similar in some of the bins during grasp. However, the similarity existed only in a small percentage bins, because the discrimination of these two objects was relatively high in the trial-wise CM which used voting method to make the final classification decision. This is also the reason why the trial-wise method always outperforms the bin-wise one, even when the bin-wise classification was not very clear. The confusions between Cylinder and Plate, and Cone to Ring were common in all the sessions, probably due to similar kinematics when grasping.

Local Field Potentials Analysis

To investigate if distinct grasp patterns also exist in local field potentials (LFPs), we showed the time-frequency plots from an example LFP channel (averaged across all the trials in one session)

for each grasp type (aligned at Light ON and Light OFF, solid vertical lines) in Figure 8. All four power spectra showed similar patterns but different intensity and phases. Both the low-frequency (0.3–15 Hz) and high-frequency (100–400 Hz) bands increased in power after Light ON (during which time the monkey held the objects and waited for Light OFF). The low-frequency bands displayed enhancement earlier and longer than high-frequency bands. These two bands then returned to baseline level of activity until the end of the trial. The 15–50 Hz frequency band (corresponding to beta and low gamma), however, decreased its power and maintained a low level of activity during reaching to grasp. Soon after Light OFF, this frequency band, along with the 50 to 100 Hz frequency band, became enhanced, leaving other frequency bands largely unchanged. This gives the impression that these frequency bands behave differently, showing sensitivity to withdraw movement rather than reaching to grasp.

Despite similarity in frequency response patterns, variation related to different grasp types was still distinguishable. In the example channel illustrated, the power of between 0.3 to 15 Hz was high when grasping cylinder, but lasted for a briefer time than for other objects. Furthermore, the bhfLFP power of cylinder and plate grasp was also higher than the other two objects. Similar results but different tuning properties were also observed for other channels in both monkeys. These data suggest that LFP modulation in the frequency domain can be further used for grasp gesture classification.

Figure 8

Using SVM classifier, we decoded the four grasp types from the 7 frequency bands of the LFP power spectrum. The averaged results of all sessions in both monkeys are shown in Figure 9. The decoding accuracy varied depending on different frequency bands used and had similar trends in

both monkeys. All the frequency bands achieved an above chance-level performance and the highest classification accuracy was obtained in the broad high frequency band in both monkeys, indicating that the broad high frequency band has the most contribution to making a difference between four grasp types. The only difference between the two monkeys was that the low-frequency band decoding accuracy for B04 was higher than B03. The middle-frequency band obtained a similar poor performance in both monkeys: during decoding period (1 second after Light ON) there was a similar low level of activity, regardless of grasp type. Thus, the LFP signal also demonstrated the grasp patterns in PMd and can also be a useful grasp decoding signal source.

Figure 9

Discussion

The present study inspected the grasp patterns in dorsal premotor cortex using both spike and local field potential signals and their reliable grasp type decoding in two monkeys. We found that, the grasp type discrimination information was encoded only during a short period soon after movement onset (i.e., during the period of *reaching*, *grasping* and beginning of *holding*) rather than along the whole time course of grasp. These evidences can further be used in practical brain machine interfaces for grasp motor prosthesis.

PMd and Dorsomedial Grasp Network

The dorsomedial pathway in cortical grasp networks, which is organized around area V6A with connection to superior parietal lobule and PMd, has been viewed as an integrating control area for reach and grasp, rather than a reach only related system (Grafton, 2010). The hub cortical area V6A neurons were found modulated to reach before (Fattori et al., 2001; 2005), however, it has been reported that V6A neurons are also modulated by the orientation of the wrist and the preshaping of the hand during reach-to-grasp actions (Fattori et al., 2009; 2010). A recent human fMRI study also demonstrated similar conclusion (Monaco et al., 2011). Together with the previous findings (Raos et al., 2004; Stark et al., 2007; Hendrix et al., 2009) and the results reported in this study that area PMd contains both reaching and grasping tuned neurons, these evidences indicate that the dorsomedial parieto-frontal pathway is essential for integrating reaching requirements with a goal-directed grasp (Galletti et al., 2003; Grafton, 2010), and may play an important role in reaching to grasp movements.

Given that PMd has a dense anatomical connection with V6A (Gamberini et al., 2009), it is putative that the grasp related information in PMd is provided by V6A. Comparing with the grasp

neurons in PMv (Murata et al., 1997; Raos et al., 2006), the PMd neurons have similar tuning properties (Raos et al., 2003; Stark et al., 2007). However, it is still unclear that the different roles of these areas for the control of grasp, because direct functional comparisons are rarely reported. It is supposed that PMd neurons are more dependent on visual information than PMv because of the discrimination ability of different grips both in light and in dark (Brochier and Umilta, 2007), and PMd neurons are more related to the grasp types, rather than individual finger movements (Raos et al., 2004). It is also deduced that PMd is more involved in preparation and selection of grip types, whereas PMv is more engaged in the control of prehension and the manipulation (Kantak et al., 2012). Furthermore, it is proposed that dorsolateral AIP–PMv stream may control the grasp according to current perceptual conditions, while the dorsomedial V6A–PMd required in fast control (Fattori et al., 2010). These hypotheses need future evidences from simultaneous recordings in both dorsomedial and ventromedial areas.

It has been widely reported that PMd is also critical for accomplishing associative memory processes between visual cues and motor outputs. Electrophysiology recordings in monkey and human revealed that PMd responded to presentation of visual cues that is associative with a particular grasp output (Kurata and Wise, 1988; Mitz et al., 1991; Chouinard et al., 2005). This involvement in conditional motor behaviors was further supported by lesion studies (Petrides, 1985; Kurata and Hoffman, 1994; Davare et al., 2006; Nowak et al., 2009) and functional imaging (Grafton et al., 1998). However, it is noteworthy that the Light ON/OFF cues used in this study are different from the associative visual cues mentioned above. The visual cues in this study were used to prompt the monkey to grasp or release the objects and the properties of the cues were always the same. The prehensile patterns adopted by the monkeys only depended on the objects to be grasped,

rather than the different visual cues (e.g., different colors, shapes, etc.).

The visual responses evoked only by the objects presentation have been observed in this study, as previous works reported (Raos et al., 2004). For example, the Neuron 94-2 from B04 shown in Fig.2 fired differently for different objects even before Light ON, during which monkey just fixate the object. After Light ON, however, there are additional modulations superimposed on the visual response, which should be due to the grasp action itself. For later analysis and decoding, we subtract the baseline firing for each object (see Methods) to eliminate the visual influence on grasp action modulation. Meanwhile, as the monkey can see the objects during the whole time course of grasp, the modulation observed can also not be due to the visual stimulation evoked by the hand or object after Light ON (Fogassi et al., 1999). Our data thus indicate that PMd is involved in the control of the hand gestures to adapt differently shaped objects during reaching to grasp actions.

Synergic and hierarchical motor control

The distinct neural patterns in PMd for different grips are demonstrated in this study, based on which the grasp types can be decoded reliably using both spike and LFPs signals. The similar grasp decoding is also reported in previous works (Stark and Abeles, 2007; Carpaneto et al., 2011; Townsend et al., 2011). So it may be reasonable to argue that grasp types, rather than individual finger kinematics, are encoded in brain as a simplified control strategy. Actually, Synergy has been proposed recently as a solution to the problem that how brain effectively controls the many DoFs of the hand movement (Santello et al., 2013). The synergy control has been demonstrated both in kinematics (Santello et al., 1998; Thakur et al., 2008) and muscular level (Brochier et al., 2004; Overduin et al., 2008). It is also believed that the synergies observed are originated from central nervous system (Holdefer and Miller, 2002; Overduin et al., 2012; Bizzi and Cheung, 2013). The

neural reduction results as shown in Figure 4, which depict the distinct grasp clusters in the same 3D space, can also be evidences for the neural synergy control.

The grasp patterns encoded in PMd are distinct but brief. As shown in Figure 5, the duration of grasp encoding only exists in a short period soon after movement onset, rather than along the whole time course of grasp. It means that the cortical signals do not encode the grasp gesture information any more during *holding* period. Nevertheless, it has been demonstrated that there are distinctive and reproducible patterns of EMG activation during grasp, and the pattern can maintain at a constant high level even during the static *holding* period (Brochier et al., 2004). We can infer that the discriminable grasp pattern existed only in EMG activities rather than in PMd cortical signals during the static *holding* period. It shows a distributed hierarchical way organized the motor nervous control systems, in which different parts encode movement at different levels of abstraction (Felleman and Van Essen, 1991). A higher level (such as premotor cortex) may only encode planning, leaving the details of movement to a lower level (such as musculature). Actually, there are also evidences showing motor synergy organized in spinal cord (Tresch et al., 1999; Hart and Giszter, 2010) and a spinal circuitry centered control scheme has been recently proposed (Santello et al., 2013).

LFP performance in grasp movement

Different LFP frequency bands power contributed diversely to the grasp types decoding. In both monkeys, the high-frequency band got the highest decoding accuracies. Similar decoding results were also found in decoding of reach and grasp kinematic parameters in primary motor cortex (Zhuang et al., 2010) and reach direction classification in both M1 and PMd (Ince et al., 2010). The highest decoding accuracy of LFP was competitive but always inferior to spike counterpart.

However, LFP was usually considered as more stable signals (Ince et al., 2010), suitable for global parameters classification (Asher et al., 2007) and with higher information in individual LFP channels (Bansal et al., 2011). Nonetheless, the beta and low gamma (around 15–50 Hz) frequency bands showed noticeable inhibition after movement onset, which is a little different from the observation in M1 and PMv (Spinks et al., 2008). In contrast, these frequency bands got enhanced during releasing the objects and withdrawing hand, which had not been reported before. The reason can be diverse, e.g. encoding of reach movement from far to near body side or encoding of attention from concentrated to rest, which need to be confirmed in future investigation.

Implications for BMIs

Decoding grasp gestures instead of individual kinematics has been demonstrated as an efficient way to reduce the computation complexity for prosthetics control in BMIs; this is due to the synergistic mechanisms involved in both natural grasp and brain control (Schieber and Santello, 2004). Stark and Abeles had successfully classified two types of grip using multiunit activity (MUA) in PMd and PMv (Stark and Abeles, 2007); Carpaneto and colleagues tested several algorithms for up to 6 grip types decoding using single neuron recording in PMv and got an accuracy of over 95% (Carpaneto et al., 2011); Townsend et al. performed online grip decoding using multiple units in PMv and AIP, which found that PMv was better suited for classification of the grip type (Townsend et al., 2011). The high classification accuracies using ensemble PMd neurons in our study also showed evidences of grasp types encoding in brain. In addition, PMd was found more suitable for prediction of future occurrence of discrete targets in reaching tasks (Hatsopoulos et al., 2004), which indicate that PMd may be used for an integrated reaching and grasp decoding.

However, most of current studies investigated synchronous (event related) decoding algorithms

(Stark and Abeles, 2007; Carpaneto et al., 2011; Townsend et al., 2011), i.e., systems in which the start trigger is required to the decoder, which is not generally available in practical circumstances. On the other hand, an asynchronous BMI can decode the continuous signal and estimate the subject's cognitive state every time bin in an unstructured manner (Aggarwal et al., 2008; Kemere et al., 2008). Our previous study demonstrated an asynchronous decoding of four grasp types and a resting state, in which both the movement states and movement onset timing could be classified accurately based on neural data without non-neural cue tips (Hao et al., 2012; 2013). In this work, the classifier models employed also worked in a bin-wise model and achieved a high accuracy according to bin-wise confusion matrix analysis, which implied an asynchronous decoding for practical BMIs.

References:

Aggarwal V, Acharya S, Tenore F, Shin HC, Etienne-Cummings R, Schieber MH, Thakor NV (2008) Asynchronous decoding of dexterous finger movements using M1 neurons. IEEE T Neur Sys Reh 16:3-14.

Asher I, Stark E, Abeles M, Prut Y (2007) Comparison of direction and object selectivity of local field potentials and single units in macaque posterior parietal cortex during prehension. J Neurophysiol 97:3684-3695.

Bansal AK, Vargas-Irwin CE, Truccolo W, Donoghue JP (2011) Relationships among low-frequency local field potentials, spiking activity, and three-dimensional reach and grasp kinematics in primary motor and ventral premotor cortices. J Neurophysiol 105:1603-1619.

Belkin M, Niyogi P (2003) Laplacian eigenmaps for dimensionality reduction and data representation. Neural Comput 15:1373-1396.

Bizzi E, Cheung VC (2013) The neural origin of muscle synergies. Front Comput Neurosci 7:51-56.

Brochier T, Umilta MA (2007) Cortical control of grasp in non-human primates. Curr Opin Neurobiol 17:637-643.

Brochier T, Spinks RL, Umilta MA, Lemon RN (2004) Patterns of muscle activity underlying object-specific grasp by the macaque monkey. J Neurophysiol 92:1770-1782.

Caminiti R, Johnson PB, Galli C, Ferraina S, Burnod Y (1991) Making arm movements within different parts of space: the premotor and motor cortical representation of a coordinate system for reaching to visual targets. J Neurosci 11:1182-1197.

Carpaneto J, Umilta MA, Fogassi L, Murata A, Gallese V, Micera S, Raos V (2011) Decoding the

activity of grasping neurons recorded from the ventral premotor area F5 of the macaque monkey. Neuroscience 188:80-94.

Chang C, Lin C (2011) LIBSVM: a library for support vector machines. ACM Transactions on Intell Sys Techn (TIST) 2:27.

Chouinard PA, Leonard G, Paus T (2005) Role of the primary motor and dorsal premotor cortices in the anticipation of forces during object lifting. J Neurosci 25:2277-2284.

Davare M, Kraskov A, Rothwell JC, Lemon RN (2011) Interactions between areas of the cortical grasping network. Curr Opin Neurobiol 21:565-570.

Davare M, Andres M, Cosnard G, Thonnard JL, Olivier E (2006) Dissociating the role of ventral and dorsal premotor cortex in precision grasping. J Neurosci 26:2260-2268.

Fattori P, Gamberini M, Kutz DF, Galletti C (2001) 'Arm-reaching' neurons in the parietal area V6A of the macaque monkey. Eur J Neurosci 13:2309-2313.

Fattori P, Kutz DF, Breveglieri R, Marzocchi N, Galletti C (2005) Spatial tuning of reaching activity in the medial parieto-occipital cortex (area V6A) of macaque monkey. Eur J Neurosci 22:956-972.

Fattori P, Breveglieri R, Marzocchi N, Filippini D, Bosco A, Galletti C (2009) Hand orientation during reach-to-grasp movements modulates neuronal activity in the medial posterior parietal area V6A. J Neurosci 29:1928-1936.

Fattori P, Raos V, Breveglieri R, Bosco A, Marzocchi N, Galletti C (2010) The dorsomedial pathway is not just for reaching: grasping neurons in the medial parieto-occipital cortex of the macaque monkey. J Neurosci 30:342-349.

Felleman DJ, Van Essen DC (1991) Distributed hierarchical processing in the primate cerebral cortex. Cereb Cortex 1:1-47.

Fogassi L, Raos V, Franchi G, Gallese V, Luppino G, Matelli M (1999) Visual responses in the dorsal premotor area F2 of the macaque monkey. Exp Brain Res 128:194-199.

Fogassi L, Ferrari PF, Gesierich B, Rozzi S, Chersi F, Rizzolatti G (2005) Parietal lobe: from action organization to intention understanding. Science 308:662-667.

Fu QG, Suarez JI, Ebner TJ (1993) Neuronal specification of direction and distance during reaching movements in the superior precentral premotor area and primary motor cortex of monkeys. J Neurophysiol 70:2097-2116.

Galletti C, Kutz DF, Gamberini M, Breveglieri R, Fattori P (2003) Role of the medial parieto-occipital cortex in the control of reaching and grasping movements. Exp Brain Res 153:158-170.

Gamberini M, Passarelli L, Fattori P, Zucchelli M, Bakola S, Luppino G, Galletti C (2009) Cortical connections of the visuomotor parietooccipital area V6Ad of the macaque monkey. J Comp Neurol 513:622-642.

Gardner EP, Ro JY, Babu KS, Ghosh S (2007) Neurophysiology of prehension. II. Response diversity in primary somatosensory (S-I) and motor (M-I) cortices. J Neurophysiol 97:1656-1670.

Grafton ST (2010) The cognitive neuroscience of prehension: recent developments. Exp Brain Res 204:475-491.

Grafton ST, Fagg AH, Arbib MA (1998) Dorsal premotor cortex and conditional movement selection: A PET functional mapping study. J Neurophysiol 79:1092-1097.

Hao Y, Chen W, Zhang S, Zhang Q, Jiang B, Zhao T, Zheng X (2012) Continuous neural decoding of grasp types for asynchronous brain machine interfaces. Conf Proc IEEE Eng Med Biol Soc 2012:6422-6425.

Hao Y, Zhang Q, Zhang S, Zhao T, Wang Y, Chen W, Zheng X (2013) Decoding grasp movement

from monkey premotor cortex for real-time prosthetic hand control. Chinese Sci Bull 58:2512-2520.

Hart CB, Giszter SF (2010) A neural basis for motor primitives in the spinal cord. J Neurosci 30:1322-1336.

Hatsopoulos N, Joshi J, O'Leary JG (2004) Decoding continuous and discrete motor behaviors using motor and premotor cortical ensembles. J Neurophysiol 92:1165.

Hendrix CM, Mason CR, Ebner TJ (2009) Signaling of grasp dimension and grasp force in dorsal premotor cortex and primary motor cortex neurons during reach to grasp in the monkey. J Neurophysiol 102:132-145.

Holdefer RN, Miller LE (2002) Primary motor cortical neurons encode functional muscle synergies. Exp Brain Res 146:233-243.

Hoshi E, Tanji J (2006) Differential Involvement of Neurons in the Dorsal and Ventral Premotor Cortex During Processing of Visual Signals for Action Planning. J Neurophysiol 95:3596-3616.

Ince NF, Gupta R, Arica S, Tewfik AH, Ashe J, Pellizzer G (2010) High accuracy decoding of movement target direction in non-human primates based on common spatial patterns of local field potentials. PLoS One 5:e14384.

Kantak SS, Stinear JW, Buch ER, Cohen LG (2012) Rewiring the brain: potential role of the premotor cortex in motor control, learning, and recovery of function following brain injury. Neurorehabil Neural Repair 26:282-292.

Keller JM, Gray MR, Givens JA (1985) A Fuzzy K-Nearest Neighbor Algorithm. IEEE T Sys, Man, Cyber 15:581.

Kemere C, Santhanam G, Yu BM, Afshar A, Ryu SI, Meng TH, Shenoy KV (2008) Detecting neural-state transitions using hidden Markov models for motor cortical prostheses. J Neurophysiol

100:2441-2452.

Kurata K, Wise SP (1988) Premotor cortex of rhesus monkeys: set-related activity during two conditional motor tasks. Exp Brain Res 69:327-343.

Kurata K, Hoffman DS (1994) Differential effects of muscimol microinjection into dorsal and ventral aspects of the premotor cortex of monkeys. J Neurophysiol 71:1151-1164.

Messier J, Kalaska JF (2000) Covariation of primate dorsal premotor cell activity with direction and amplitude during a memorized-delay reaching task. J Neurophysiol 84:152-165.

Mitz AR, Godschalk M, Wise SP (1991) Learning-dependent neuronal activity in the premotor cortex: activity during the acquisition of conditional motor associations. J Neurosci 11:1855-1872.

Monaco S, Cavina-Pratesi C, Sedda A, Fattori P, Galletti C, Culham JC (2011) Functional magnetic resonance adaptation reveals the involvement of the dorsomedial stream in hand orientation for grasping. J Neurophysiol 106:2248-2263.

Murata A, Fadiga L, Fogassi L, Gallese V, Raos V, Rizzolatti G (1997) Object representation in the ventral premotor cortex (area F5) of the monkey. J Neurophysiol 78:2226-2230.

Nicolelis MA, Dimitrov D, Carmena JM, Crist R, Lehew G, Kralik JD, Wise SP (2003) Chronic, multisite, multielectrode recordings in macaque monkeys. Proc Natl Acad Sci USA 100:11041-11046.

Nowak DA, Berner J, Herrnberger B, Kammer T, Gron G, Schonfeldt-Lecuona C (2009) Continuous theta-burst stimulation over the dorsal premotor cortex interferes with associative learning during object lifting. Cortex 45:473-482.

Overduin SA, D'Avella A, Roh J, Bizzi E (2008) Modulation of muscle synergy recruitment in primate grasping. J Neurosci 28:880-892.

Overduin SA, D'Avella A, Carmena JM, Bizzi E (2012) Microstimulation activates a handful of muscle synergies. Neuron 76:1071-1077.

Petrides M (1985) Deficits in non-spatial conditional associative learning after periarcuate lesions in the monkey. Behav Brain Res 16:95-101.

Raos V, Franchi G, Gallese V, Fogassi L (2003) Somatotopic organization of the lateral part of area F2 (dorsal premotor cortex) of the macaque monkey. J Neurophysiol 89:1503-1518.

Raos V, Umilta MA, Gallese V, Fogassi L (2004) Functional properties of grasping-related neurons in the dorsal premotor area F2 of the macaque monkey. J Neurophysiol 92:1990-2002.

Raos V, Umilta MA, Murata A, Fogassi L, Gallese V (2006) Functional properties of grasping-related neurons in the ventral premotor area F5 of the macaque monkey. J Neurophysiol 95:709-729.

Rizzolatti G, Matelli M (2003) Two different streams form the dorsal visual system: anatomy and functions. Exp Brain Res 153:146-157.

Santello M, Flanders M, Soechting JF (1998) Postural hand synergies for tool use. J Neurosci 18:10105-10115.

Santello M, Baud-Bovy G, Jorntell H (2013) Neural bases of hand synergies. Front Comput Neurosci 7:23-37.

Schieber MH, Santello M (2004) Hand function: peripheral and central constraints on performance. J Appl Physiol 96:2293-2300.

Spinks RL, Kraskov A, Brochier T, Umilta MA, Lemon RN (2008) Selectivity for grasp in local field potential and single neuron activity recorded simultaneously from M1 and F5 in the awake macaque monkey. J Neurosci 28:10961-10971.

Stark E, Abeles M (2007) Predicting movement from multiunit activity. J Neurosci 27:8387-8394.

Stark E, Asher I, Abeles M (2007) Encoding of reach and grasp by single neurons in premotor cortex is independent of recording site. J Neurophysiol 97:3351-3364.

Stark E, Globerson A, Asher I, Abeles M (2008) Correlations between groups of premotor neurons carry information about prehension. J Neurosci 28:10618-10630.

Suner S, Fellows MR, Vargas-Irwin C, Nakata GK, Donoghue JP (2005) Reliability of signals from a chronically implanted, silicon-based electrode array in non-human primate primary motor cortex. IEEE T Neur Sys Reh 13:524-541.

Thakur PH, Bastian AJ, Hsiao SS (2008) Multidigit movement synergies of the human hand in an unconstrained haptic exploration task. J Neurosci 28:1271-1281.

Thomson DJ (2000) Multitaper analysis of nonstationary and nonlinear time series data. Nonlinear and nonstationary signal processing:317-394.

Townsend BR, Subasi E, Scherberger H (2011) Grasp movement decoding from premotor and parietal cortex. J Neurosci 31:14386-14398.

Tresch MC, Saltiel P, Bizzi E (1999) The construction of movement by the spinal cord. Nat Neurosci 2:162-167.

Van der Maaten L, Postma EO, Van Den Herik HJ (2009) Dimensionality reduction: A comparative review. J Mach Learn Res 10:1-41.

van Nuenen BF, Kuhtz-Buschbeck J, Schulz C, Bloem BR, Siebner HR (2012) Weight-specific anticipatory coding of grip force in human dorsal premotor cortex. J Neurosci 32:5272-5283.

Verhagen L, Dijkerman HC, Grol MJ, Toni I (2008) Perceptuo-motor interactions during prehension movements. J Neurosci 28:4726-4735.

Wise SP, Boussaoud D, Johnson PB, Caminiti R (1997) Premotor and parietal cortex: corticocortical connectivity and combinatorial computations. Annu Rev Neurosci 20:25-42.

Zhang QS, Zhang SM, Hao YY, Zhang H, Zhu J, Zhao T, Zhang J, Wang Y, Zheng X, Chen W (2012) Development of an invasive brain-machine interface with a monkey model. Chinese Sci Bull 57:2036-2045.

Zhuang J, Truccolo W, Vargas-Irwin C, Donoghue JP (2010) Decoding 3-D reach and grasp kinematics from high-frequency local field potentials in primate primary motor cortex. IEEE T Biomed Eng 57:1774-1784.

Legends

Figure 1. Experimental setup and task. (A) Experimental setup showing monkey reaching to grasp an object on a panel. Neural signals are recorded during grasp task. Subpanel shows the four target objects and corresponding grasp gestures used in this study. (B) Placement of the PMd (and MI) arrays in monkey B04, which located at the ventrorostral part of caudal PMd (F2vr). (C) The time sequence of a single trial with stages of movement (above) and external events: visual light on for grasp initiation and light off for release. A drop of water is given as reward at the end of each trial.

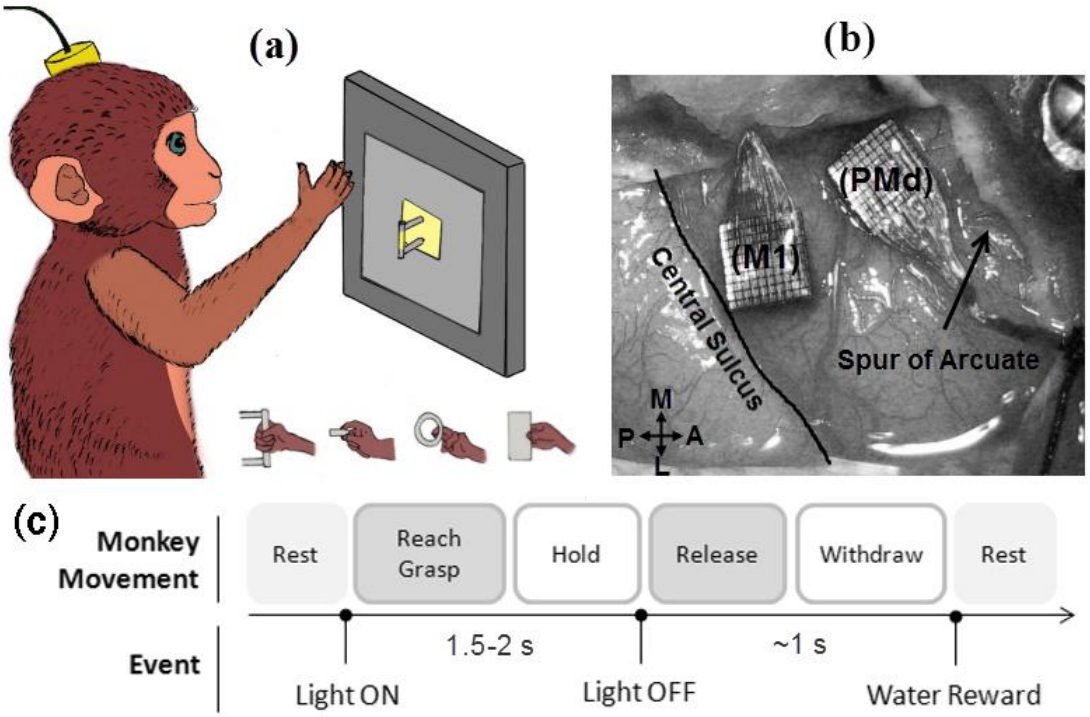

Figure 2. Neural response of eight example neurons (four from B03 and four from B04) during reaching to grasp movement. The top six neurons are modulated by different grasp types, while the bottom two neurons responded to grasp but did not show differential response to different objects. For each neuron, the firing rate during grasping each of the four different objects was averaged separately across all the trials in one session. Each curve was aligned to the timing of Light ON (left)

and Light OFF (right) (indicated by the two vertical lines in each panel), leaving one break point in the middle. Neuron 77-2 means the 2nd unit from channel 77 and so on. Based on the video recorded, the four upward arrows in the top two panels indicate the approximate onset of reach (R), grasp (G), hold (H) and release (Rls) .

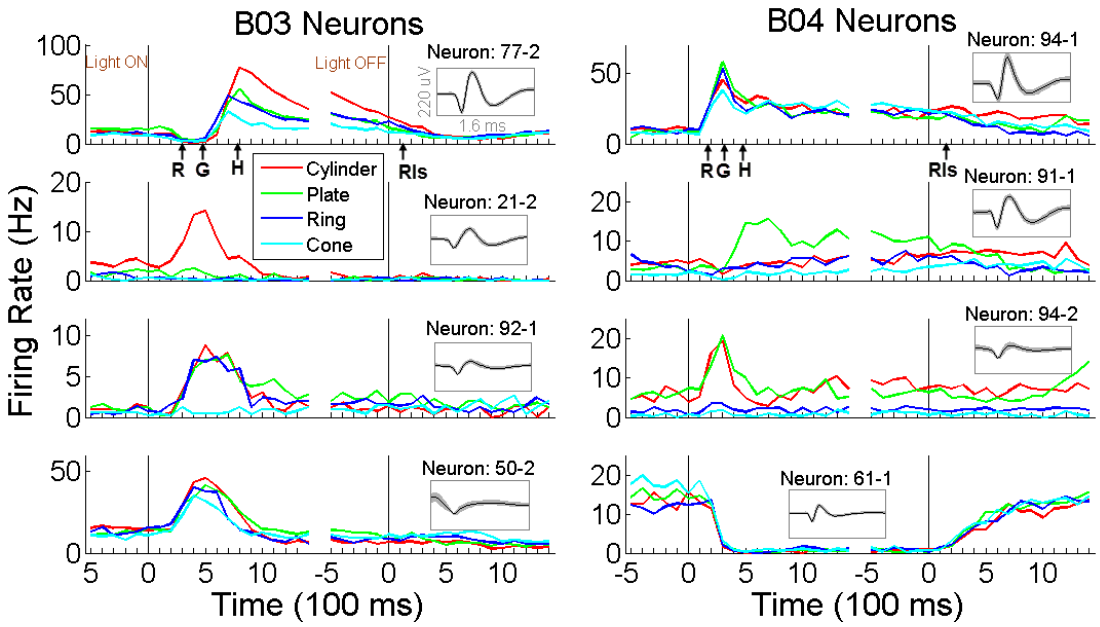

Figure 3. Pair wise distance matrices for grasp of different objects from monkey B03 (A) and B04 (B). Pseudocolor represents standardized Euclidian distance between each pair of neural firing vectors. The value of the color is indicated by the colorbar at right; the highest values (dark red) mean the lowest level of similarity. Numbers 1, 2, 3 and 4 along the axes in the matrices (10 trials each) represent neural vectors from grasping cylinder, ring, cone and plate, respectively. Each matrix was averaged across all the bins in 1 second after Light ON event.

Figure 4. The LE reduced neuronal firing patterns in 3D space from two representative sessions in Monkey B03 (A) and B04 (B). Each line represents the whole time course of a grasp trial. Different colors mean different objects as shown in the legend plot. The violet rectangle indicates the averaged position of Light ON and the adjacent arrow shows the time lapsing

direction. LE1, LE2 and LE3 represent the reduced 3D space coordinates.

Figure 5. Percentage of correctly sorted objects (Cs) as a function of movement time course. The Cs was calculated based on hierarchical clustering analysis and averaged across all 8 sessions conducted in each monkey. The results were also aligned to Light ON (left) and Light OFF (right) as in figure 2. The period, during which the Cs values are significantly different from baseline, is illustrated in the plot for each monkey (B03: pink; B04: blue).

Figure 6. Decoding results using spike signals and its dependencies. (A) Session-wise classification accuracy using four decoding models (different colors) in monkey B03 and B04. The averaged accuracies were also tabled in the plot for each classifier and each monkey. (B) The performance along the time course of grasp using a sliding time window decoding approach. Different time windows from 300 to 900 ms were tested. The results in the plot were averaged from one representative session of monkey B03. (C) Classification accuracy as a function of training trials from two example sessions in B03 and B04. (D) Decoding performance as a function of the number of neurons used in the classifier. Each neuron number tested in the plot was random selected and the results were averaged 50 times. SVM decoding model was used for the results in (B), (C) and (D).

Figure 7. The trial-wise and bin-wise confusion matrices of decoding results for one representative session of monkey B04. These matrices described the prediction errors of individual objects made by the SVM classifier. The performance of the classifier for each target object is

represented by the percentage number label in the corresponding squares, which is also depicted by gray shading

Figure 8. Time-frequency plots of single-channel LFP power from Monkey B04 for the four grasp types. The representative LFP power relative to baseline was plotted as a function of time and frequency, averaged across all the trials in one session and doubly aligned at the Light ON and OFF as the two solid vertical lines shown in each plot. The vertical dashed line indicates the separation between the two aligns. The frequency axis was logarithmically transferred to make the low and middle frequency bands expanded and clear. The LFP power spectrum patterns of four grasp types displayed distinguishable time-varying features.

Figure 9. The decoding accuracy of seven frequency bands of LFPs in Monkey B03 and B04. The broad high frequency band (200 - 400 Hz) produced the highest decoding accuracy in both monkeys. Asterisk indicated the frequency bands whose decoding accuracies are significant different with the lowest one in each monkey.

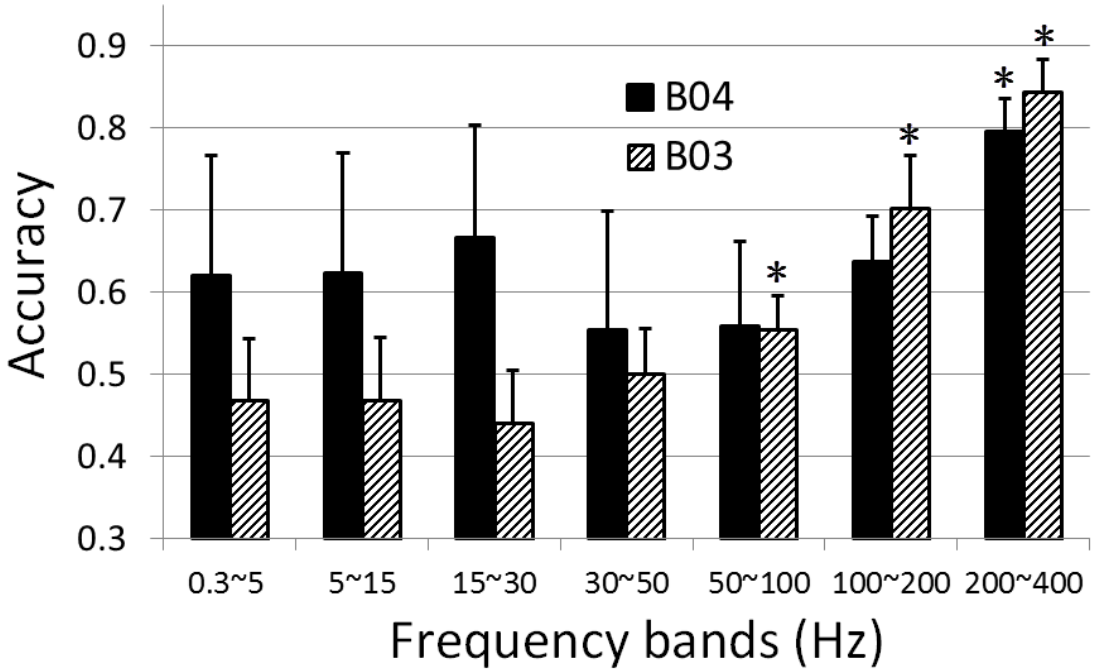
0.9
0.8
0.7
0.6
0.5
0.4
0.3
Accuracy
B04
B03
*
*
*
*
0.3~5
5~15
15~30
30~50
50~100
100~200
200~400
Frequency bands (Hz)